Pharmacological Reports 71 (2019) 13–23

Contents lists available at ScienceDirect

Pharmacological Reports

journal homepage: www.elsevier.com/locate/pharep

Original article

Antitumor effects of berberine against EGFR, ERK1/2, P38 and AKT in MDA-MB231 and MCF-7 breast cancer cells using molecular modelling and *in vitro* study

Parham Jabbarzadeh Kaboli[a], Melody Pui-Yee Leong[b], Patimah Ismail[a,*], King-Hwa Ling[a,b]

[a] Department of Biomedical Science, Faculty of Medicine and Health Sciences, Universiti Putra Malaysia, Selangor, Malaysia
[b] Genetics and Regenerative Medicine Research Centre, Faculty of Medicine and Health Sciences, Universiti Putra Malaysia, Selangor, Malaysia

ARTICLE INFO

Article history:
Received 6 October 2017
Received in revised form 14 July 2018
Accepted 31 July 2018
Available online 1 August 2018

Keywords:
Berberine
AKT
EGFR
Breast cancer
Molecular modelling

ABSTRACT

Background: Berberine is an alkaloid plant-based DNA intercalator that affects gene regulation, particularly expression of oncogenic and tumor suppressor proteins. The effects of berberine on different signaling proteins remains to be elucidated. The present study aimed to identify the effects of berberine against key oncogenic proteins in breast cancer cells.
Methods: Molecular docking and molecular dynamics simulations were used for EGFR, p38, ERK1/2, and AKT. The effects of berberine and lapatinib on MAPK and PI3K pathways in MDA-MB231 and MCF-7 cells were evaluated using immunoflorescence assays, and the amounts of phosphorylated kinases were compared to total kinases after treating with different concentrations of berberine.
Results: Simulations showed berberine accurately interacted with EGFR, AKT, P38, and ERK1/2 active sites *in silico* (scores = -7.57 to -7.92 Kcal/mol) and decreased the levels of active forms of corresponding enzymes in both cell lines; however, berberine binding to p38 showed less stability. Cytotoxicity analysis indicated that MDA-MB231 cells were resistant to berberine compared to MCF-7 cells [72 h IC_{50} = 50 *versus* 15 μM, respectively). Also, lapatinib strongly activated AKT but suppressed EGFR in MDA-MB231 cells. The activity of EGFR, AKT, P38, and ERK1/2 were affected by berberine; however, berberine dramatically reduced EGFR and AKT phosphorylation.
Conclusion: By way of its multikinase inhibitory effects, berberine might be a useful replacement for lapatinib, an EGFR inhibitor which can cause acquired drug resistance in patients.

Introduction

Breast cancer is the most frequently diagnosed cancer in women and the second most common cancer worldwide. The membranous protein epidermal growth factor receptor (EGFR) is a crucial biomarker of breast cancer, and dysregulation of the EGFR-mitogen-activated protein kinase (MAPK) signaling pathway is common in this disease [1]. The effects of EGFR are mediated by overactivation of MAPK and extracellular signal-regulated kinase (ERK), and the basal levels of ERK are known to be higher in tumor cells [2].

The protein p38 MAPK (p38) has also been shown to be relevant to the motility of breast cancer cells by affecting proteins involved in actin dynamics [2]. While the MAPK pathway is primarily activated by EGFR, it also crosstalks with the phosphatidylinositol-3-kinase (PI3K)/RAC-α serine/threonine protein kinase (AKT) pathway, and both pathways interact with apoptosis signaling [3]. Inhibition of the MAPK pathway has been shown to activate PI3K/AKT signaling to induce resistance to EGFR inhibitors [4,5]. Hence, finding both AKT and EGFR inhibitors could potentially lead to more effective cancer treatments [5,6].

Berberine (BBR) is a nitogenous cyclic compound with a structure that is highly similar to that of intercalating agents [3]. BBR has also been shown to have inhibitory effects on PI3K/AKT in MDA-MB231 and MCF-7 breast cancer cells [7]. As the effects of BBR against various signaling proteins differ in a number of cell lines, the immediate targets of BBR in breast cencer cells remain unknown. In the current study, the anti-oncogenic effects of BBR against EGFR, ERK1/2, p38, and AKT were examined in breast cancer cells. Using computational molecular modelling and dynamics simulations, the inhibitory effects of BBR against these proteins were predicted, then select proteins were examined further *in vitro*.

* Corresponding author.
E-mail addresses: admin@parhamscience.com (P. Jabbarzadeh Kaboli), meleonpy@gmail.com (M.P.-Y. Leong), patimah@upm.edu.my (P. Ismail), lkh@upm.edu.my (K.-H. Ling).

https://doi.org/10.1016/j.pharep.2018.07.005
1734-1140/

Materials and methods

Docking and molecular dynamics (MD) simulations setup

BBR (PubChem CID: 2353; DrugBank ID: DB04115; ZINC ID: 03779067), lapatinib (PubChem CID: 208908), a p38 inhibitor (PubChem CID: 56951457), and adenosine triphosphate (ATP; PubChem CID: 15126) as the normal substrate were used for *in silico* studies. Using the RCSB protein data bank [8], three crystal structures were downloaded for EGFR, AKT, p38, ERK kinase domain (Table 1), and all generated ligands were docked to all crystals. To perform molecular modelling and dynamics simulations, configurations were used according to a previously published protocol [9]. To normalize docking data based on molecular properties and bioavailability, binding efficiency indices (BEIs) were calculated as explained by Abad-Zapatero [10–12].

In vitro *chemicals and reagents*

MDA-MB231 and MCF-7 cells were grown in 25-cm^2 flasks with RPMI-1640 media (R8758, Sigma, USA) supplemented with fetal bovine serum (F7524, Sigma) and penicillin-streptomycin (P0781, Sigma). Cells were treated with epidermal growth factor (E41271MG, Sigma), and then collected using a phosphate-buffered saline tablet (P4417, Sigma) and trypsin-EDTA solution (T3924, Sigma). A TACS Annexin V-FITC Apoptosis Detection kit (4830-01-K, Trevigen) and 3-(4,5-dimethyl-2-thiazolyl)-2,5-diphenyl-2H-tetrazolium bromide (MTT) assay (M5655, Sigma) were used to assess cell death. BBR (B3251) and lapatinib (CDS022971) were obtained from Sigma-Aldrich, Canada and USA, respectively. Human phospho (p)-EGF R/ErbB1 (Y1068) [KCB1095], p-ERK1 (T202/Y204)/ERK2 (T185/Y187) [KCB1018], p-p38 MAPK (T180/Y182) [KCB869], and p-AKT kinase (S473) [KCB887] kits for cell-based enzyme-linked immunosorbent assay (ELISA) were purchased from R&D Systems. p-Akt1/2/3 (Ser 473) [SC-101629], p-EGFR (F-3), mouse monoclonal immunoglobulin G (IgG)-1 (SC-377547), actin (Sc-1616), goat anti-mouse IgG-horseraddish peroxidase (Sc-2005), and donkey anti-goat IgG-horseraddish peroxidase (Sc-2020) antibodies used for gel electrophoresis and Western blot were obtained from Santa Cruz Biotechnology, Inc. (USA); the prestained protein marker (02525) was purchased from Nacalai Tesque (Japan). Clarity Western Substrate (170-5060, Bio-Rad), Turbo™ PVDF Midi membranes (170-4157), Mini-PROTEAN® TGX™ precast gels (456–9033), and Laemmli buffer (161-0737) were purchased from Bio-Rad.

Cytotoxicity and apoptosis assays

An MTT (3-(4,5-dimethylthiazol-2-yl)-2,5-diphenyltetrazolium bromide) assay was used to assess the cytotoxicity of BBR and lapatinib treatment. MTT and apoptosis assays were performed based on a standard protocol [9]. Flow cytometry was used to assess the presence of apoptosis using a FACSCanto II machine. Propidium iodide and annexin V-FITC were used to determine the level of apoptotic cell death. For both assays, six 96-well plates were seeded with 5000 cells/well for each cell line then treated with different concentrations of BBR or lapatinib at serial concentrations of 0, 3.125, 6.25, 12.5, 25, 50, and 100 μM. Triplicate wells were used for each concentration. GraphPad Prism 7 was used to plot the MTT results. For each concentration, the experiment was performed as triplicate, then Kolmogorov-Smirnov normality and *t*-tests were done to determine whether the results were significant.

The enzyme-linked immunosorbent assay (ELISA)

Cell-based ELISA kits were used according to the manufacturer's instructions. Phosphorylated and total proteins were detected in MCF-7 and MDA-MB231 cells following BBR treatment. *In vitro* experiments were analyzed using a Student's *t*-test, and significance was set at $P = 0.05$.

Sodium dodecyl sulfate-polyacrylamide gel electrophoresis and Western blotting

Concentrations of isolated proteins were set to 15 μg/lane. For Western blotting, p-AKT, AKT, p-EGFR, and EGFR antibodies were diluted 1:200 in blocking buffer (1% bovine serum albumin). Bands were expected to be at 200 and 60 KDa for EGFR and AKT, respectively. Proteins were transfered onto membranes within 10 min. Gel electrohproesis and blotting were conducted using the manufacturer's protocols (Bio-Rad Bulletins 6376 and 5871) and Springer Protocols [13]. Phosphorylated protein were analyzed in duplicate. Lapatinib and dimethylsulfoxide (DMSO) were used as positive and negative controls, respectively. Bio-Rad Quantity One 4.6.6 was used to quantify bands.

Results

Effect of BBR and lapatinib on cellular morphology

Fig. 1 shows the combined effect of 50–100 μM BBR and lapatinib on cancer cell proliferation and integrity. MCF-7 cells treated with BBR showed different morphologies with different treatment durations (24–72 h) [Fig. 1A-F]. After 24-h treatment, various cytoplasmic white vesicles were observed (Fig. 1E) that were not present in untreated MCF-7 cells. This result shows an increase in vesicular trafficking in response to BBR treatment. In contrast, MDA-MB231 cells had dendritic appendages while attached to flask surface with BBR treatment (Fig. 1G-J). Over time, BBR treatment caused MDA-MB231 cell detachment from the flask and produced spherical cell shapes; the presence of white, cytoplasmic vesicles was rare. While 100 μM BBR triggered necrosis of MCF-7 cells, the same concentration and treatment

Table 1
Pdb files of targets obtained from RCSB Protein Data Bank and related information.

Protein	PDB ID	Phenotype	Resolution (nm)	R-value work	R-value free
EGFR	1m14	Wild-type	0.26	0.238	0.286
	4i1z	Mutated	0.3	0.187	0.227
	4i23	Wild-type	0.28	0.226	0.279
ERK1/2	4n0s	Wild-type	0.18	0.154	0.189
	4xj0	Wild-type	0.258	0.208	0.244
	4zzm	Mutated	0.189	0.207	0.254
p38 MAPK	3u8w	Wild-type	0.215	0.234	0.255
	4aa4	Wild-type	0.23	0.211	0.255
	4aac	Wild-type	0.25	0.230	0.305
AKT-1	3mv5	Mutated (S473D)	0.247	0.200	0.282
	3mvh	Mutated (S473D)	0.201	0.178	0.230

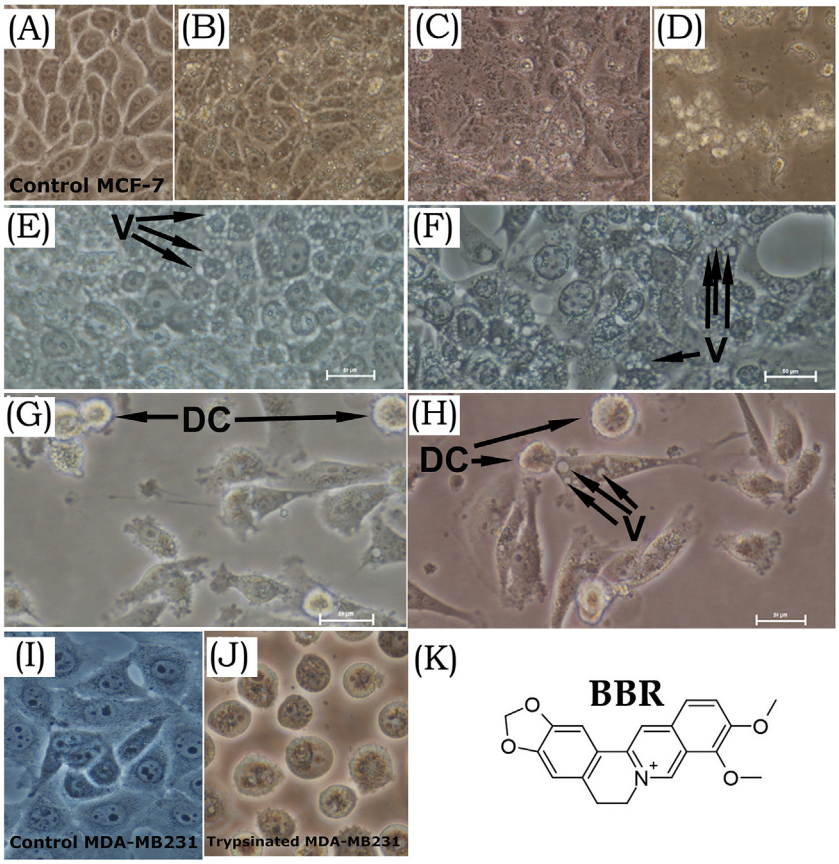

Fig. 1. Effects of BBR on MCF-7 and MDA-MB231 cells. Untreated **(A)**, lapatinib-treated [100 μM] **(B)**, and BBR-treated [100 μM] **(C)** MCF-7 cells after 48 h. **(D)** Combined lapatinib and BBR-treated (both 50 μM) MCF-7 cells after 48 h. **(E)** 100 μM BBR-treated MCF-7 cells after 48 **(E)** and 72 h **(F)**. BBR-treated (100 μM) MDA-MB231 cells after 48 **(G)** and 72 h **(H)**. Untreated **(I)** and untreated and trypsinized **(J)** MDA-MB231 cells. **(K)** BBR chemical structure. V: vesicles; DC: detached cells. 40X objective was used. Scale bar: 50 μm.

duration resulted in MDA-MB231 cell detachment as well as a degree of resistance to BBR.

BBR and lapatinib cytotoxicity

The cytotoxicity of serial concentrations of BBR after 24, 48, and 72 h of treatment were assed by MTT assay, and quarter, half, and three-quarter maximal inhibitory concentrations (IC_{25}, IC_{50}, and IC_{75}, respectively) were measured for each cell line (Table 2). MCF-7 cells had lower IC_{25}, IC_{50}, and IC_{75} values than MDA-MB231 cells, whereby IC values decreased as time increased (Fig. 2A-D). The IC_{50} value for 72-h BBR-treated MCF-7 cells was 15 μM. In contrast, MDA-MB231 cells had a higher IC_{25}, IC_{50}, and IC_{75}. The concentration-response curve for lapatinib *versus* BBR on MDA-

Table 2
T-test results of cytotoxicity of berberine.

Cells	Statistics	72h	48h	24h
MCF-7	IC25	5 μM	10 μM	125 μM
	IC50	15 μM	70 μM	165 μM
	IC75	45 μM	>100 μM	–
	Mean	56.69	69.28	72.04
	Std. Deviation	29.59	21.32	35.54
	Std. Error of Mean	13.23	8.704	12.57
	95% CI of discrepancy	19.96 to 93.43	46.9 to 91.65	42.33 to 101.8
	t, df	t = 4.285 df = 4	t = 7.959 df = 5	t = 5.733 df = 7
	P value (two tailed)	0.0128	0.0005	0.0007
	Significant (α = 0.05)	Yes	Yes	Yes
MDA-MB231	IC25	5 μM	20 μM	120 μM
	IC50	50 μM	115 μM	185 μM
	IC75	95 μM	–	–
	Mean	51.38	70.29	85.78
	Std. Deviation	31.12	22.69	21.34
	Std. Error of Mean	11.76	8.576	8.71
	95% CI of discrepancy	22.6 to 80.16	49.3 to 91.27	63.39 to 108.2
	t, df	t = 4.368 df = 6	t = 8.196 df = 6	t = 9.848 df = 5
	P value (two tailed)	0.0047	0.0002	0.0002
	Significant (α = 0.05)	Yes	Yes	Yes

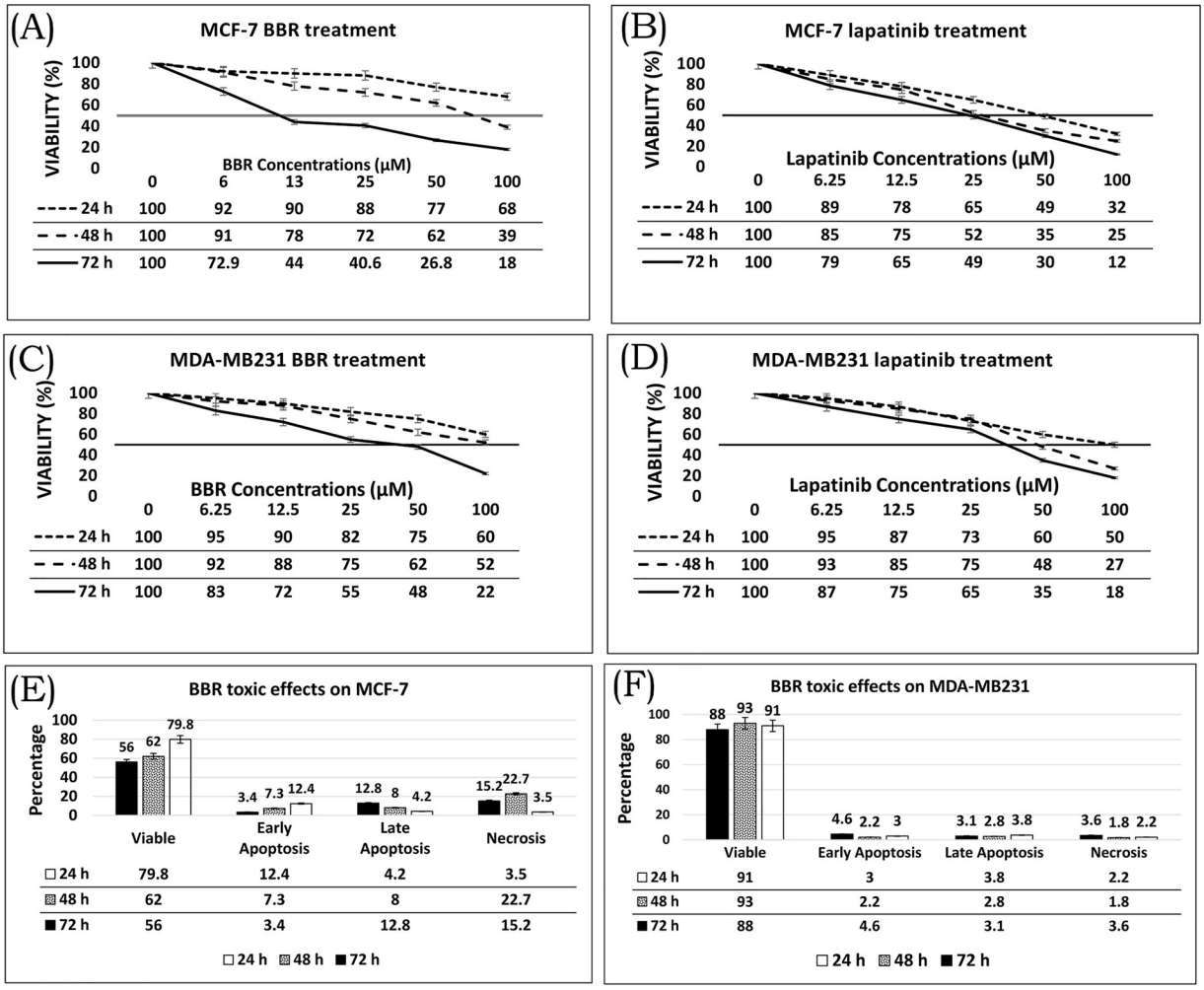

Fig. 2. Cytotoxic effects of BBR on MCF-7 and MDA-MB231 cells. **(A)** Concentration-viability curves of BBR- **(A)** and lapatinib-treated **(B)** MCF-7 cells over time. Concentration-viability curves of BBR- **(C)** and lapatinib-treated **(D)** MDA-MB231 cells over time. MCF-7 **(E)** and MDA-MB231 **(F)** cell death at different time points; drug concentrations = 50 μM. The results confirm MDA-MB231 resistance to BBR as there is greater viability and IC_{50} values for MDA-MB231 *versus* MCF-7 cells. Horizontal lines (A–D) are IC_{50} lines.

MB231 cells demonstrates the remarkable effect of lapatinib during 24-h treatment.

BBR-induced apoptotic and necrotic cell death

Flow cytometry was used to assess whether cell death occurred by apoptosis or necrosis. After 24-h BBR treatment, MCF-7 cells underwent early and late stages of apoptosis (Fig. 3). The number of apoptotic and necrotic MCF-7 cells at different treatment durations depicted in Fig. 2E-F shows changes in the percentage of dead cells. These results indicate MCF-7 cells were sensitive to BBR; because early apoptosis was apparently too short, the affected cells became necrotic and/or entered late-stage apoptosis soon after. In agreement with their higher IC_{50}, there were fewer necrotic *versus* than apoptotic (both early- and late-stage) MDA-MB231 cells after 24-h BBR treatment (Fig. 3F-H). Both cell types, however, exhibited both concentration- and time-dependent inhibition by BBR.

Molecular modelling of BBR interactions with EGFR, AKT, ERK1/2, and p38

Molecular modelling was performed against several crystals to predict and compare the inhibitory effects of BBR on EGFR, AKT, ERK1/2, and p38 and the average results were computed (Table 3). The parameters computed for targets demonstrated that the average binding energy and inhibition constant (K_i) for the four kinases were very close, with an energy range between -7.78 and -7.22 Kcal/mol for AKT and EGFR, respectively. The average K_i also changed from 2 μM for AKT to 5.73 μM for EGFR. The average K_i for ERK and p38 were 4.32 and 3.73 μM, respectively. pK_i calculations showed that BBR was predicted to have inhibitory effect on all four kinases, with AKT having the highest pK_i (5.70). BEIs were also calculated to optimize the thermodynamics of docking based on the physicochemical properties of BBR (Table 3). The results indicated that the highest BEI and NSEI belong to AKT (nBEI = 7.10; NSEI = 1.14), and the lowest belong to EGFR (nBEI = 6.64; NSEI = 1.05). Because the differences in BEI and NSEI values among the proteins are relatively small, BBR is predicted to inhibit all four proteins.

The structure of BBR has four rings providing π-interactions with neighboring residues, depending on the residue structure. Comparison of the interpolated charge (approximately 0.00) and hydrophobicity (approximately 3.00) of EGFR (Fig. 4A-D) showed its binding cavity provides suitable hydrophobicity for BBR to entry. The Lys745 residue plays a major role through hydrogen bonding and hydrophobic interactions. Lysine has a long chain involved with alkyl interactions and an amino side group able to form hydrogen bonds. Met793, Leu792, and Leu718 are also important for interactions in the binding cavity (Fig. 4B). In

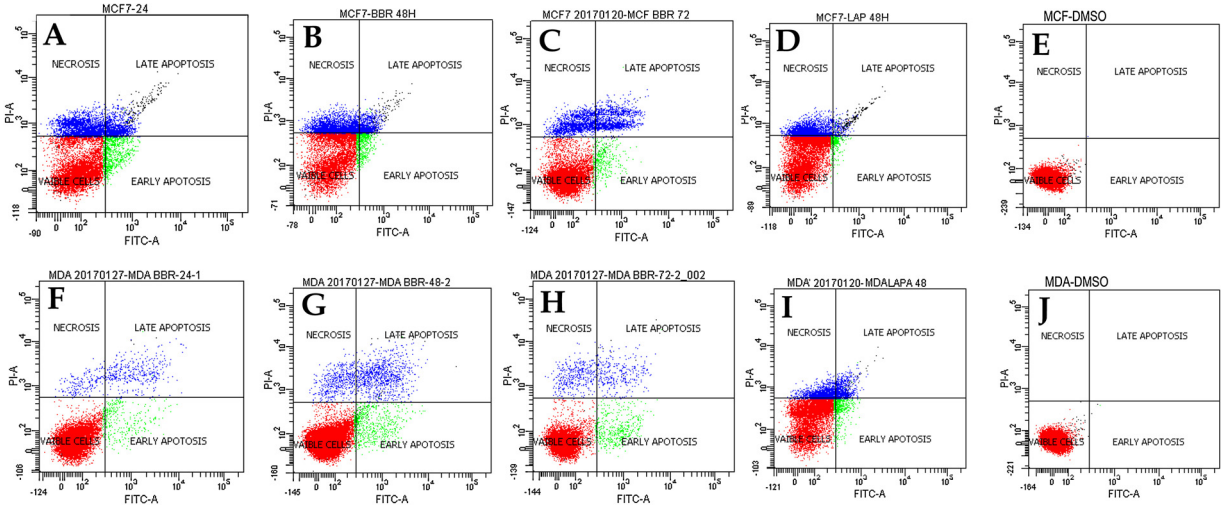

Fig. 3. Apoptosis analysis in MCF-7 and MDA-MB231 cells. Flow cytometric analysis of apoptosis in MCF-7 cells treated with 50 μM BBR for 24 **(A)**, 48 **(B)**, and 72 h **(C)**. MCF-7 cells treated with 50 μM lapatinib **(D)** or 1% DMSO [control] **(E)** for 48 h. Flow cytometric analysis of apoptosis in MDA-MB231 cells treated with BBR (50 μM) for 24 **(F)**, 48 **(G)**, and 72 h **(H)**. MDA-MB231 cells treated with 50 μM lapatinib **(I)** or 1% DMSO [control] (J) for 48 h. The number of viable MDA-MB231 cells was much higher than MCF-7 cells, demonstrating the sensitivity of MCF-7 cells to BBR.

Table 3
Docking information for berberine docked to p38 MAPK, ERK1/2, EGFR, and AKT1.

Target	Min. E. (kcal/mol)	Average E. (kcal/mol)	Min. Ki (μM)	Average Ki (μM)	pKi[1] (M)	nBEI[2]	NSEI[3]
p38	−7.6	−7.416	2.68	3.73	5.43	6.83	1.09
ERK1/2	−7.92	−7.51	1.57	4.32	5.36	6.76	1.07
EGFR	−7.57	−7.22	2.81	5.73	5.24	6.64	1.05
AKT1	−7.83	−7.78	1.830	2.00	5.70	7.10	1.14

1. pKi = -LogKi; **2**. nBEI = pKi + Log[nha], Binding efficiency index based on the logarithmic number of heavy atoms; **3**. NSEI = pKi/(polar atoms), Surface efficiency index based on the integer number of polar atoms.

contrast, Asp292 causes the AKT binding cavity to have a range of hydrophobicity (from -3.00–3.00) [Fig. 4E-G]. The AKT binding cavity also has two residues with electronegative side chains (Thr291 and Met227) and lacks lysine, making AKT's binding cavity more polar than EGFR's. Val164 also plays a major role in the hydrophobic interactions of the AKT binding cavity (Table 4).

Kinases have similar structures containing two lobes (C and N). The C-lobe is rich in α-helices, while the N-lobe is rich in β-sheets and has only two α-helices. In Fig. 5A-B, BBR was clearly bound to a cleft located between the N- and C-lobes of ERK. β-Sheets located at the N-lobe play a major role in BBR-ERK interactions. Lys114, Lys84, and Asp167 are polar residues involved in both hydrogen bonding and hydrophobic interactions, and Met108 and Leu156 play a role in hydrophobic interactions. In order to determine the stability of target, root-mean-square (RMS) deviation (RMSD) and RMS fluctuation (RMSF) were computed using MD simulations (Fig. 5C-D). The average RMSD computed was as low as 0.25 nm for BBR-ERK interactions (Fig. 5C).

Molecular modelling and MD simulations of p38 predicted that Lys53 and Asp168 are involved in hydrogen bonding with BBR (Fig. 5E-F). These residues are comparable to Lys114 and Asp167 of ERK as previously discussed. Therefore, ERK1/2 and p38 as cytoplasmic kinases form very similar globular structures that are targeted by BBR. For these *in silico* experiments, three different crystals of each enzyme were used. p38 was also found to hydrophobically interact with BBR through Thr106, Ala51, and Val38. The MD results confirmed that the average deviation among α-carbons was less than 0.30 nm (Fig. 5G). In order to verify p38 results, adenosine triphosphate and one p38 inhibtor [14] were used as controls and their molecular interactions compared with BBR (not shown here). The average RMSD for the p38 inhibitor docked to p38 was 0.22 nm, showing a stronger interaction than with BBR. We observed unfavorable bond formation between BBR and p38 (Fig. 5E), as the average RMSD and RMSF were higher than with the other three enzymes studied herein. Therefore, the inhibitory effects of BBR on p38 are predicted to be lower than for AKT, EGFR, and ARK1/2.

Effect of BBR on total and phosphorylated ERK1/2, AKT, p38, and EGFR

ELISA was performed to comfirm the results of *in silico* studies. Both total and phosphorylated enzymes were detected at the same time to normalize the results for each well. On the other hand, the level of normalized phosphorylated kinases demonstrates the inhibitory effects of BBR on corresponding targets. Total kinase detection revealed that total EGFR, p38, ERK1/2, and AKT activities were reduced in both MCF-7 and MDA-MB231 cells. While total p38 and ERK1/2 levels remained steady after a slight reduction (Fig. 6), total EGFR levels decreased dramatically; total AKT levels did not decrease as significantly as EGFR. Apart from EGFR, none of the other total kinase levels decreased more than 50%. The reduction of total protein may be due to the interaction of BBR with proteins involved in transcription and translation. All results relative to total kinases levels were significant based on *t*- and *p*-values ($\alpha = 0.05$). Fig. 6 demonstrates the Optical Densities of (ODs) and Relative Flourescent Units (RFUs) of each total and phosphorylated kinases in different concentrations.

Using this technique, the effects of BBR on phosphorylation of Tyr1068 (EGFR), Ser473 (AKT), Thr180 and Tyr182 (p38), Thr202 and Tyr204 (ERK1), and Thr185 and Tyr187 (ERK2) were also

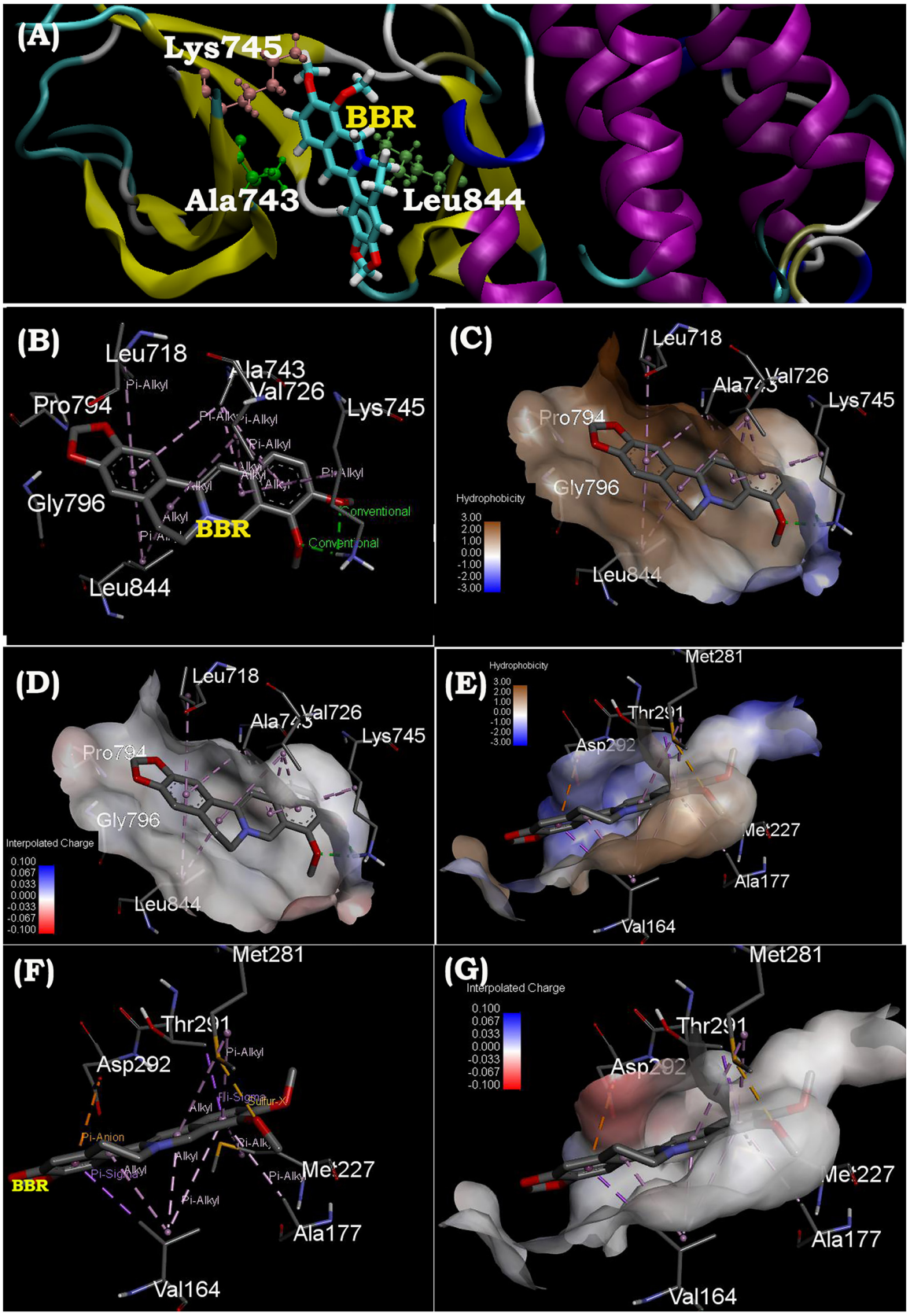

Fig. 4. Molecular modelling of BBR inhibition of EGFR and AKT. **(A)** BBR-docked EGFR structure depicted by Visual Molecular Dynamics. **(B)** BBR and EGFR interactions. **(C)** Hydrophobicity of surrounding residues for BBR-EGFR interactions. **(D)** Analysis of interpolated charges of surrounding residues for BBR-EGFR interactions. BBR effectively binds Lys745 of EGFR. **(E)** Hydrophobicity of surrounding residues for BBR-AKT interactions. **(F)** In BBR-AKT interactions, Val164 is more important for alkyl-π interactions between BBR and AKT. **(G)** Analysis of interpolated charges of surrounding residues for BBR-AKT interactions. PDB IDs: 3mvh (AKT) and 4i23 (EGFR). Interactions were analyzed by Discovery Studio Visualizer.

Table 4
Interaction analysis of docked berberine to ERK2, p38, EGFR, and AKT.

Molecular system	Residues	Interactions	Length of interactions (nm)
ERK2/BBR	Met108	H-Bond	0.227
	Gly34 (CO), Ala35 (N)	Amide-π stacked interaction	0.466
	Lys54	Alkyl interaction	0.5 and 0.511
	Val39	π-Alkyl interaction	0.496
	Val39	Alkyl interaction	0.496 and 0.476
	Ala52	π-Alkyl interaction	0.413
	Ala52	Alkyl interaction	0.464
P38/BBR	Val38	π- Alkyl interaction	0.473
	Val38	Alkyl interaction	0.493
	Ala51	π- Alkyl interaction	0.416
	Ala51	Alkyl interaction	0.366
	Leu108	π- Sigma interaction	0.365
	Ala157	Alkyl interaction	0.439
	Lys53	π- Alkyl interaction	0.511
	Gly110	Unfavorable interaction	Clash between two polar oxygens (0.268)
EGFR/BBR	Lys745	H-bond	0.205 and 0.310
	Lys745	π- Alkyl interaction	0.396
	Lys745	Alkyl interaction	0.486
	Val726	π- Alkyl interaction	0.505
	Val726	Alkyl interaction	0.444 and 0.489
	Ala743	π- Alkyl interaction	0.459 and 0.533
	Leu718	π- Alkyl interaction	0.511
	Leu844	Alkyl interaction	0.450
	Leu844	π- Alkyl interaction	0.506
AKT/BBR	Arg4	π- Cation interaction	0.290
	Thr291	H-bond	0.284
	Val164	Alkyl interaction	0.402
	Val164	π- Sigma interaction	0.363 and 0.386
	Met281	π interaction	0.532
	Ala177	π- Alkyl interaction	0.535
	Leu156	π- Alkyl interaction	0.487
	Met227	π- Alkyl interaction	0.536
	Asp292	π- Anion interaction	0.418

determined. Overall, BBR treatment caused phosphorylation levels to decrease (Fig. 6B,D). Comparison of p-EGFR in both cell types shows a large decrease in p-EGFR levels in MDA-MB231 cells but slight decrease in MCF-1 cells with BBR treatment. Its feasible that rapid changes in p-EGFR may cause greater changes to MDA-MB231 cell membrane structure, leading to their rapid detachment and apoptosis as discussed above. On the other hand, because MCF-7 cells would retain higher levels of p-EGFR and remain attached. While p-p38, p-AKT, and p-ERK1/2 levels were decreased by BBR, their IC_{50} values were higher than that of p-EGFR. In MCF-7 cells, p-AKT, p-ERK1/2, and p-p38 had similar rates of reduction which were similar to those in MDA-MB231 cells. Therefore, it is possible that alterations in p-EGFR inhibition play a role in cell death and determine how sensitive cancer cells are to BBR. In BBR-treated MDA-MB231 cells where p-EGFR is lacking, the levels of ERK1/2 and p38 should also be decreased as a result of EGFR reduction; however, we observed that p38 remained active while EGFR declined in both cell lines.

Effect of BBR on p-EGFR and p-AKT in MDA-MB231 cells

Western blotting was performed to further examine the effects of BBR on phosphorylation of EGFR and AKT in MDA-MB231 cells treated with 12.5, 25, and 50 μM BBR; 50 μM lapatinib; and 1% DMSO as a control (Fig. 7). To compare and quantify bands, the adjusted volume of the intensity per mm^2 was used (adjusted volume = total volume - background volume). p-AKT levels were reduced in BBR-treated MDA-MB231 cells to approximately one-sixth of the control. This experiment surprisingly demonstrates that lapatinib-treated MDA-MB231 cells have 4-times greater activation of AKT than control cultures. p-EGFR activation was reduced to approximately one-third that of the control with either BBR or lapatinib. These results indicate that BBR can effectively inhibit both AKT and EGFR. On the other hand, lapatinib increased the level of p-AKT, which might be a mechanism by which MDA-MB231 cells become resistant to lapatinib.

Discussion

BBR has proapoptotic and anticancer activities in several cell lines [15]. Considering a number of mutated proteins are involved in cancer development, the response of cells depends on the type of mutations and the surrounding environment. BBR is an intercalating agent that can attach to adenylyl groups in DNA and RNA and has been shown to affect gene expression in breast cancer cells [3,16–23]. However, because BBR can bind both oncogenic and housekeeping mRNAs, it can be toxic to normal cellular activity. In the present study, we performed *in silico* studies to predict the overall effects of BBR on four selected oncoproteins then examined its effects further *in vitro*. Overall, we found that BBR concentrations greater than 50 μM were highly toxic to both MDA-MB231 and MCF-7 cancer cell lines.

Using molecular modelling and dynamics studies, we predicted that BBR targets p38, ERK, EGFR, and AKT. This was confirmed by our *in vitro* results which showed that BBR decreased the levels p-p38, p-EGFR, p-AKT, and p-ERK1/2. Accordingly, the activation of all four kinases was decreased, among which a plunge was observed for EGFR with lower concentrations of BBR. Previous studies have shown that BBR affects MAPK signaling pathways mostly by indirect inhibition [4,24,25]. In addition, BBR has been shown to downregulate EGFR [26,27] most likely by suppressing other proteins involved in gene regulation, such as nuclear factor-κB [28]. In contrast, indirect EGFR inhibition by BBR has been shown *via* activation of Cbl in colon tumor cells. BBR has also been shown to inhibit EGFR in prostate cancer [29] and decrease AKT levels in highly metastatic MDA-MB231 breast cancer cells

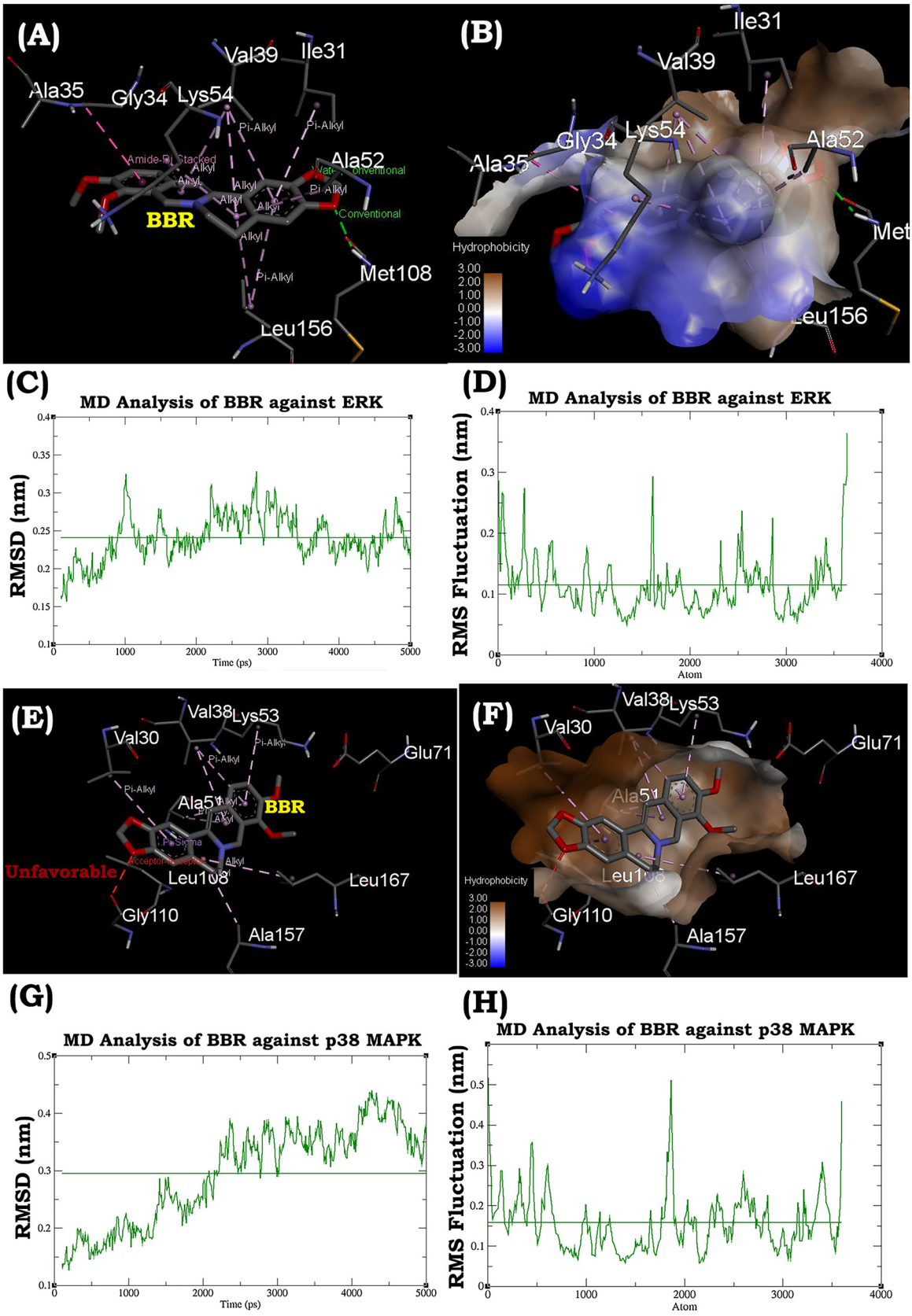

Fig. 5. Molecular modelling of BBR inhibition of ERK1/2 and p38. **(A)** BBR-docked ERK2 interaction showing involvement of Lys54 and surrounding hydrophobic residues. **(B)** Hydrophobicity of surrounding residues for BBR-ERK2 interactions. Average RMSD **(C)** and RMSF **(D)** of BBR against ERK2 over time. **(E)** BBR and p38 interactions. Similar to ERK2, Lys53 and surrounding hydrophobic residues were involved in BBR-p38 interactions, but an unfavorable bond was detected in BBR-p38 docking. **(F)** Hydrophobicity of surrounding residues for BBR-p38 interactions. Average RMSD **(G)** and RMSF **(H)** of BBR against p38 over time. The average RMSD is <0.3 nm, showing binding stability. Comparison of ERK2 and p38 molecular dynamics (MD) results showed ERK2 is more stable. The dynamic movement observable in **(G)** and average RMSF seen in **(H)** are higher than those in **(C)** and **(D)**. PDB IDs: 4n0s (ERK) and 3u8w (p38). Interactions and MD were visualized by Discovery Studio Visualizer and Grace, respectively.

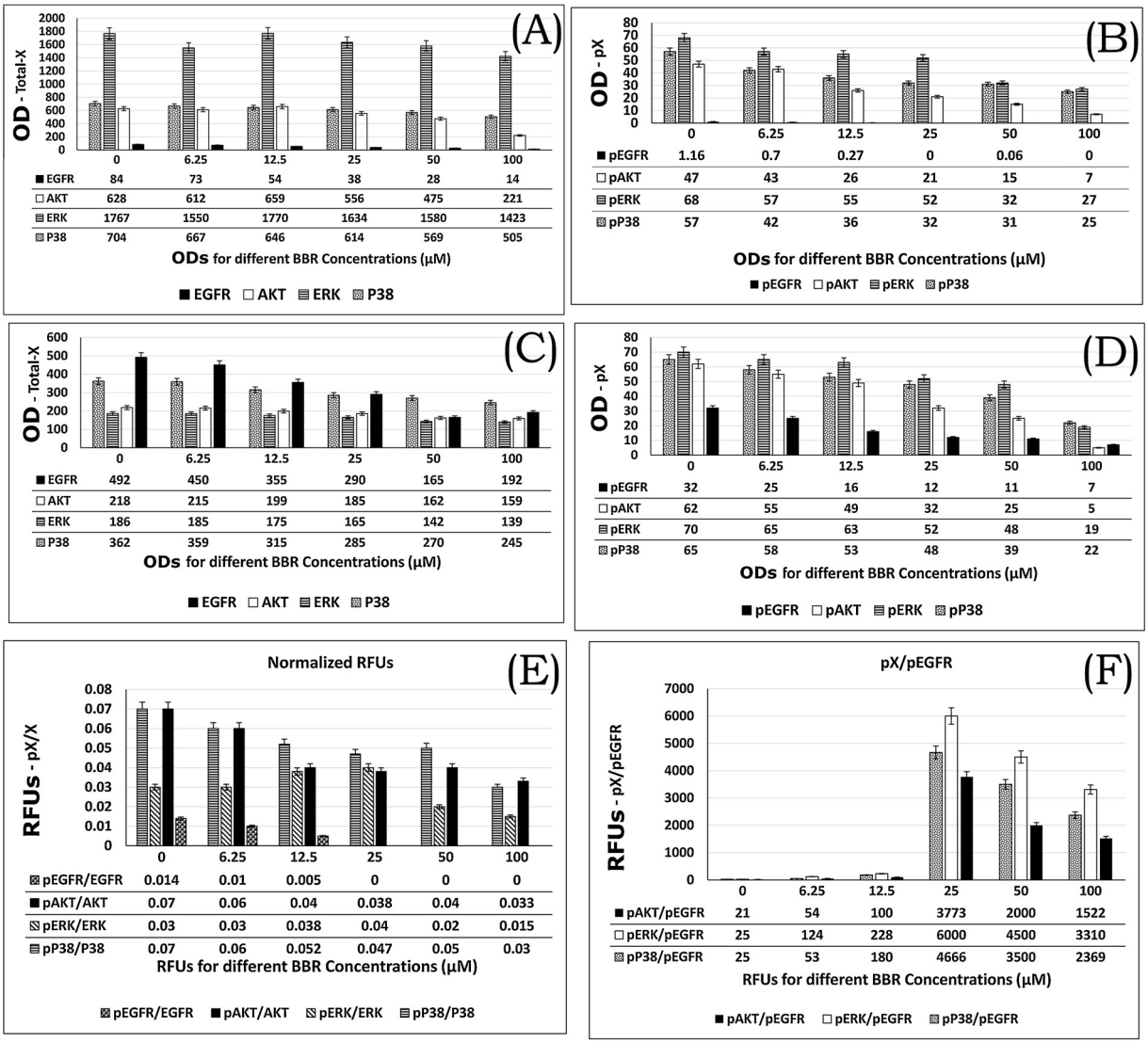

Fig. 6. Effects of BBR on AKT, EGFR, p38, and ERK1/2. **(A–D)** Concentration-response graphs of different BBR concentrations on each kinase after 48-h treatment. Total and phosphorylated kinases were detected in the same well. Total **(A)** and phosphorylated **(B)** kinase Optical Density (OD) in BBR-treated MDA-MB231 cells. Total **(C)** and phosphorylated **(D)** kinase ODs in BBR-treated MCF-7 cells. **(E)** Relative Fluorescent Units (RFUs) in BBR-treated MDA-MB231 cells. Normalized RFUs were calculated as the ODs read for phosphorylated kinases divided by the RFU read for total kinases in the same well. **(F)** Graph generated based on the ratios of p-ERK, p-p38, and p-AKT RFUs to p-EGFR RFUs in MDA-MB231 cultures after 48 h of BBR treatment. Activation percentages were calculated by dividing the average percentage of activated protein in treated cells by the average percentage of activated protein in untreated (healthy) cells.

[7]. Therefore, the effects of BBR on other proteins or pathways regulating EGFR activity, such as Cbl, should be considered. The current study also showed that BBR may act as a moderate inhibitor of p38 and ERK1/2; however, the decrease observed in p-p38 and p-ERK1/2 levels may partly be related to a reduction in p-EGFR and upstream signaling proteins, such as BRAF and KRAS [30–32].

Untreated MDA-MB231 cells express normal levels of EGFR and AKT [33], whereas MCF-7 cells display EGFR overactivation and increased levels of p-AKT [34]. AKT suppresses caspase-dependent apoptosis and activates necroptosis and caspase-independent programmed cell death by tumor necrosis factor-α activation [23]. PI3K/AKT signaling is involved with vesicular trafficking, and AKT is a key regulator of this pathway [35]. Herein, we observed that BBR affects p-EGFR and p-AKT in MDA-MB231 cells more so than MCF-7 cells. Therefore, the difference between the morphological structures of MDA-MB231 and MCF-7 cells after BBR treatment was likely associated with the higher level of AKT activity in BBR-treated MCF-7 cells.

MDA-MB231 is a triple-negative breast cancer cell line known to be resistant to tyrosine kinase inhibitors, such as lapatinib [36]. While BBR reduced the level of EGFR in MDA-MB231 cells in the present study, the level of EGFR in these cells was dramatically lower than that in MCF-7 cells. Although reduced EGFR expression is a known feature of MDA-MB231 cells [36], other alternative signaling proteins, such as nuclear factor erythroid 2-related factor 2, downstream of EGFR signaling have also been implicated in MDA-MB231 cellular resistance to tyrosine kinase inhibitors [37, 38]. We detected a decrease in the level of EGFR and an increase in the level of p-AKT in MDA-MB231 cells that may explain lapatinib's effects on AKT. However, BBR successfully suppressed both EGFR and AKT in MDA-MB231 cells. The mechanisms by which MDA-MB231 cells respond to lapatinib and its effect on p-AKT requires further examination. In contrast to MDA-MB-231 cells, MCF-7 cells express Her2, Her3, and EGFR [39]. Her3 and Her2 interact with EGFR to transduce EGF signaling to MAPK and downstream targets [3]. EGFR activation in MCF-7 cells is supported by the Her2 receptor. Hence, both EGFR expression and the IC50 of BBR for

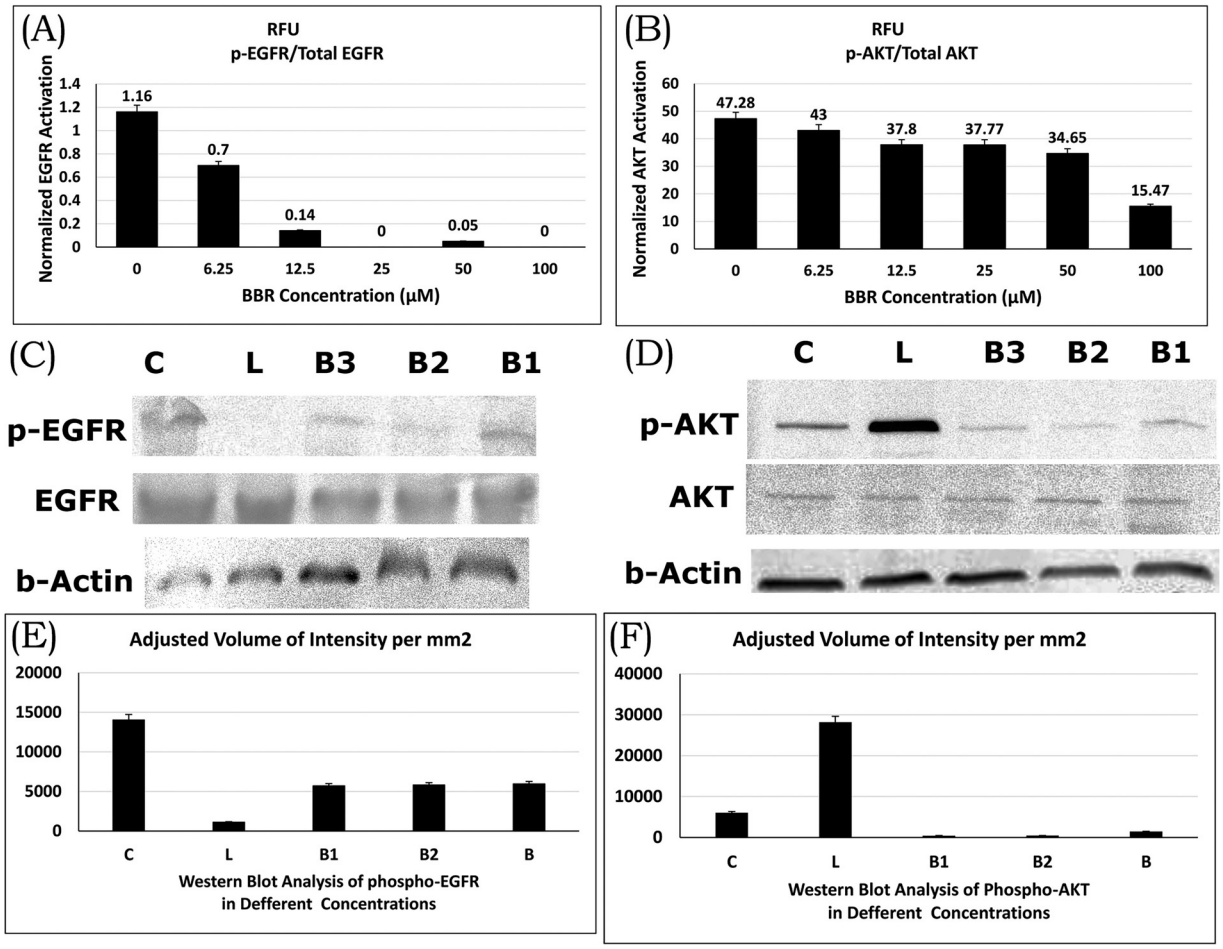

Fig. 7. Effects of BBR on p-EGFR and p-AKT in MDA-MB231 breast cancer cells. BBR concentration-response of p-EGFR **(A)** and p-AKT **(B)** in MDA-MB231 cells. Western blot of p-EGFR **(C)** and p-AKT **(D)** levels in MDA-MB231 cells treated with BBR or lapatinib. Densitometric analysis of p-EGFR **(E)** and p-AKT **(F)** levels in MDA-MB231 cells treated with BBR or lapatinib. MDA-MB231 cells are resistant to tyrosine kinase inhibitors, such as lapatinib. In contrast to BBR, lapatinib dramatically increased AKT activation in MDA-MB231 cells, but suppressed EGFR activation (phosphorylation). β-Actin was used for normalization. Adjusted volume = (total volume – background volume). For each BBR concentration, the level of p-EGFR, p-AKT, and β-actin were detected using the same blot but different duplicate lanes labeled B1-B3 (12.5, 25, and 50 μM, respectively), L (50 μM), and C (1% DMSO).

p-EGFR were increased in the present study. In contrast, MDA-MB231 cells lack Her2 activity, making p-EGFR more sensitive, decreasing the IC_{50} of BBR for p-EGFR in MDA-MB231 cells dramatically. However, the overall survival rate of MDA-MB231 cells treated with BBR was higher, and overall IC_{50} values at different times were higher than those in MCF-7 cells.

In cases of acquired resistance to lapatinib, BBR can reverse this resistance in MCF-7 cells [40]. BBR greatly sensitizes breast cancer cells by suppressing AKT and human Smoothened receptor [9]. AKT inhibitors also sensitize tumor cells to stimulate apoptosis [41]. Although lapatinib inhibited EGFR, we found MDA-MB231 cells were resistant to lapatinib by overactivation of AKT. Since MDA-MB231 cells are tyrosine kinase inhibitor-resistant cells [37], this outcome shows a new hope for overcoming lapatinib resistance in cancer treatment. Thus, using AKT inhibitors in combination with lapatinib is suggested for the future studies. Our findings demonstrate that BBR has potential antitumor activity in breast cancer cells; however, further studies using animal models with induced breast cancer are required.

Conclusions

In the present study, kinases in the MAPK signaling pathway were inhibited by BBR. We concluded that BBR targets kinase domains of EGFR and AKT. By targeting AKT, BBR also affects the PI3K signaling pathway. Based on the current *in vitro* and *in silico* studies, BBR was determined to have moderate activity against other targets (p38 and ERK1/2). Therfore, finding more potent BBR derivatives with lower K_i's is suggested.

Conflict of interest

None of the authors have any conflict of interest.

Funding

Authors declare that no external funding was received for this study.

Acknowledgements

The authors would like to thank Professor Dr. Johnson Stanslas of the Pharmatherapeutics Laboratory at Department of Medicine, Universiti Putra Malaysia (UPM) for his helpful comments on the research design, as well as his kind gift of the MCF-7 and MDA-MB231 cell lines and some other materials used in this study. We are also grateful to Ms. Loh Pei Qi, a Bio-Rad product specialist, and Ms. Heng Kai Yen, a Bio-Rad application specialist, for their supportive maintenance and assistance.

References

[1] Lee E.-J., Oh S-Y, Sung M-K. Luteolin exerts anti-tumor activity through the suppression of epidermal growth factor receptor-mediated pathway in MDA-MB-231 ER-negative breast cancer cells. Food Chem Toxicol 2012;50:4136–43, doi:http://dx.doi.org/10.1016/j.fct.2012.08.025.

[2] Squires MS, Hudson EA, Howells L, Sale S, Houghton CE, Jones JL, et al. Relevance of mitogen activated protein kinase (MAPK) and phosphotidylinositol-3-kinase/protein kinase B (PI3K/PKB) pathways to induction of apoptosis by curcumin in breast cells. Biochem Pharmacol 2003;65:361–76, doi:http://dx.doi.org/10.1016/S0006-2952(02)01517-4.

[3] Jabbarzadeh Kaboli P, Rahmat A, Ismail P, Ling KH. Targets and mechanisms of berberine, a natural drug with potential to treat cancer with special focus on breast cancer. Eur J Pharmacol 2014;740:584–95, doi:http://dx.doi.org/10.1016/j.ejphar.2014.06.025.

[4] Refaat A, Abdelhamed S, Saiki I, Sakurai H. Inhibition of p38 mitogen-activated protein kinase potentiates the apoptotic effect of berberine/tumor necrosis factor-related apoptosis-inducing ligand combination therapy. Oncol Lett 2015;1907–11, doi:http://dx.doi.org/10.3892/ol.2015.3494.

[5] Kirouac DC, Du JY, Lahdenranta J, Overland R, Yarar D, Paragas V, et al. Computational modeling of ERBB2 - amplified breast cancer identifies combined ErbB2 / 3 blockade as superior to the combination of MEK and AKT inhibitors. Sci Signal 2013;6:, doi:http://dx.doi.org/10.1126/scisignal.2004008 ra68.

[6] Pavlopoulou A, Oktay Y, Vougas K, Louka M, Vorgias CE, Georgakilas AG. Determinants of resistance to chemotherapy and ionizing radiation in breast cancer stem cells. Cancer Lett 2016;380:485–93, doi:http://dx.doi.org/10.1016/j.canlet.2016.07.018.

[7] Kuo HP, Chuang TC, Tsai SC, Tseng HH, Hsu SC, Chen YC, et al. Berberine, an isoquinoline alkaloid, inhibits the metastatic potential of breast cancer cells via Akt pathway modulation. J Agric Food Chem 2012;60:9649–58, doi:http://dx.doi.org/10.1021/jf302832n.

[8] Berman HM. The past and future of structure databases. Curr Opin Biotechnol 1999;10:76–80, doi:http://dx.doi.org/10.1016/S0958-1669(99)80014-7.

[9] Kaboli PJ, Bazrafkan M, Ismail P, Ling KH. Molecular modelling of berberine derivatives as inhibitors of human smoothened receptor and hedgehog signalling pathway using a newly developed algorithm on anti-cancer drugs. Recent Pat Anticancer Drug Discov 2017;12:384–400, doi:http://dx.doi.org/10.2174/1574892812666170929131247.

[10] Abad-Zapatero C, Champness EJ, Segal MD. Alternative variables in drug discovery : promises and challenges. Futur Med Chem 2014;6:577–93, doi:http://dx.doi.org/10.4155/fmc.14.16.

[11] Abad-Zapatero C, Blasi D. Ligand efficiency indices (LEIs): more than a simple efficiency yardstick. Mol Inform 2011;30:122–32, doi:http://dx.doi.org/10.1002/minf.201000161.

[12] Abad-Zapatero C. Ligand efficiency indices for drug discovery: towards an atlas-guided paradigm. Elsevier Science; 2013 ISBN: 978-0-12-404635-1.

[13] Desai S, Dworecki BR, Nlend MC. Direct immunodetection of antigens within the precast polyacrylamide gel. In: Kurien BT, Scofield RH, editors. Detection of blotted protein. Springer Press; 2015. p. 101–14, doi:http://dx.doi.org/10.1007/978-1-4939-2718-0_12 Online ISBN: 978-1-4939-2718-0.

[14] Herberich B, Jackson C, Wurz R, Pettus L, Sherman L, Liu Q, et al. Identification of triazolopyridazinones as potent p38alpha inhibitors. Bioorg Med Chem Lett 2012;22:1226–9, doi:http://dx.doi.org/10.1016/j.bmcl.2011.11.067.

[15] Sun Y, Xun K, Wang Y, Chen X. A systematic review of the anticancer properties of berberine, a natural product from Chinese herbs. Anticancer Drugs 2009;20:757–69, doi:http://dx.doi.org/10.1097/CAD.0b013e328330d95b.

[16] Wen CJ, Wu LX, Fu LJ, Yu J, Zhang YW, Zhang X, et al. Genomic screening for targets regulated by berberine in breast cancer cells. Asian Pac J Cancer Prev 2013;14:6089–94, doi:http://dx.doi.org/10.7314/APJCP.2013.14.10.6089.

[17] Giri P, Kumar GS. Specific binding and self-structure induction to poly(A) by the cytotoxic plant alkaloid sanguinarine. Biochim Biophys Acta 2007;1770:1419–26, doi:http://dx.doi.org/10.1016/j.bbagen.2007.05.005.

[18] Wang N, Zhu M, Wang X, Tan HY, Tsao S, wah, et al. Berberine-induced tumor suppressor p53 up-regulation gets involved in the regulatory network of MIR-23a in hepatocellular carcinoma. Biochim Biophys Acta 2014;1839:849–57, doi:http://dx.doi.org/10.1016/j.bbagrm.2014.05.027.

[19] Mahata S, Bharti AC, Shukla S, Tyagi A, Husain SA, Das BC. Berberine modulates AP-1 activity to suppress HPV transcription and downstream signaling to induce growth arrest and apoptosis in cervical cancer cells. Mol Cancer 2011;10(39), doi:http://dx.doi.org/10.1186/1476-4598-10-39.

[20] Liu C, Liu S, Wang Y, Wang S, Zhang J, Li S, et al. Synthesis, cytotoxicity, and DNA-binding property of berberine derivatives. Med Chem Res 2014;23:1899–907, doi:http://dx.doi.org/10.1007/s00044-013-0796-9.

[21] Islam MM, Kumar GS. Small molecule-RNA interaction: spectroscopic and calorimetric studies on the binding by the cytotoxic protoberberine alkaloid coralyne to single stranded polyribonucleotides. Biochim Biophys Acta 2009;1790:829–39, doi:http://dx.doi.org/10.1016/j.bbagen.2009.05.015.

[22] Jarzembowski JA, Rajagopalan LE, Shin HC, Malter JS. The 5'-untranslated region of GM-CSF mRNA suppresses translational repression mediated by the 3' adenosine-uridine-rich element and the poly(A) tail. Nucleic Acids Res 1999;27:3660–6, doi:http://dx.doi.org/10.1093/nar/27.18.3660.

[23] Nikoletopoulou V, Markaki M, Palikaras K, Tavernarakis N. Crosstalk between apoptosis, necrosis and autophagy. Biochim Biophys Acta - Mol Cell Res 2013;1833:3448–59, doi:http://dx.doi.org/10.1016/j.bbamcr.2013.06.001.

[24] Wang J, Yang S, Cai X, Dong J, Chen Z, Zhang S, et al. Berberine inhibits EGFR signaling and enhances the antitumor effects of EGFR inhibitors in gastric cancer. Oncotarget 2016;7:76076–86, doi:http://dx.doi.org/10.18632/oncotarget.12589.

[25] Wang J, Peng Y, Liu Y, Yang J, Ding N, Tan W. Berberine, a natural compound, suppresses hedgehog signaling pathway activity and cancer growth. BMC Cancer 2015;15(595), doi:http://dx.doi.org/10.1186/s12885-015-1596-z.

[26] Liu Q, Xu X, Zhao M, Wei Z, Li X, Zhang X, et al. Berberine induces senescence of human glioblastoma cells by downregulating the EGFR-MEK-ERK signaling pathway. Mol Cancer Ther 2015;14:355–63, doi:http://dx.doi.org/10.1158/1535-7163.MCT-14-0634.

[27] Wang L, Berne BJ, Friesner RA. Correction for Wang et al., Ligand binding to protein-binding pockets with wet and dry regions. Proc Natl Acad Sci 2012;109:, doi:http://dx.doi.org/10.1073/pnas.1207504109 9220-9220.

[28] Luqman S, Pezzuto JM. NFkB: a promising target for natural products in cancer chemoprevention. Phyther Res 2010;24:949–63, doi:http://dx.doi.org/10.1002/ptr.3171.

[29] Huang Z, Zheng H, Wang W, Wang Y, Zhong L, Wu J, et al. Berberine targets epidermal growth factor receptor signaling to suppress prostate cancer proliferation in vitro. Mol Med Rep 2014;2125–8, doi:http://dx.doi.org/10.3892/mmr.2014.2929.

[30] McCubrey JA, Abrams SL, Stadelman K, Chappell WH, LaHair M, Ferland RA, et al. Targeting signal transduction pathways to eliminate chemotherapeutic drug resistance and cancer stem cells. Adv Enzyme Regul 2010;50:285–307, doi:http://dx.doi.org/10.1016/j.advenzreg.2009.10.016.

[31] Burgeiro A, Gajate C, Dakir EH, Villa-Pulgarín JA, Oliveira PJ, Mollinedo F. Involvement of mitochondrial and B-RAF/ERK signaling pathways in berberine-induced apoptosis in human melanoma cells. Anticancer Drugs 2011;22:507–18, doi:http://dx.doi.org/10.1097/CAD.0b013e32834438f6.

[32] Jabbarzadeh Kaboli P, Ismail P, Ling KH. Molecular modeling, dynamics simulations, and binding efficiency of berberine derivatives: a new group of RAF inhibitors for cancer treatment. PLoS One 2018;13(3), doi:http://dx.doi.org/10.1371/journal.pone.0193941 e0193941.

[33] Kathryn JC, Sireesha VG, Stanley L. Triple Negative Breast Cancer Cell Lines: One tool in the search for better treatment of triple negative breast cancer Triple Negative Breast Cancer cell Lines: one tool in the search for better treatment of triple negative breast cancer. Breast Dis 2012;32:35–48, doi:http://dx.doi.org/10.3233/BD-2010-0307.

[34] Sarvaiya HA, Yoon JH, Lazar IM. Proteome profile of the MCF7 cancer cell line: a mass spectrometric evaluation. Rapid Commun Mass Spectrom 2006;20:3039–55, doi:http://dx.doi.org/10.1002/rcm.2677.

[35] Giussani P, Brioschi L, Bassi R, Riboni L, Viani P. Phosphatidylinositol 3-kinase/AKT pathway regulates the endoplasmic reticulum to golgi traffic of ceramide in glioma cells: a link between lipid signaling pathways involved in the control of cell survival. J Biol Chem 2009;284:5088–96, doi:http://dx.doi.org/10.1074/jbc.M808934200.

[36] Bellizzi A, Greco MR, Rubino R, Paradiso A, Forciniti S, Zeeberg K, et al. The scaffolding protein NHERF1 sensitizes EGFR-dependent tumor growth, motility and invadopodia function to gefitinib treatment in breast cancer cells. Int J Oncol 2015;46:1214–24, doi:http://dx.doi.org/10.3892/ijo.2014.2805.

[37] Wang X, Sun Z, Villeneuve NF, Zhao F, Li Y, Chen W, et al. Nrf2 enhances resistance of cancer cells to chemotherapeutic drugs, the dark side of Nrf2. Carcinogenesis 2008;29:1235–43, doi:http://dx.doi.org/10.1093/carcin/bgn095.

[38] Menegon S, Columbano A, Giordano S. The dual roles of NRF2 in cancer. Trends Mol Med 2016;22:578–93, doi:http://dx.doi.org/10.1016/j.molmed.2016.05.002.

[39] Fitzgerald TL, Lertpiriyapong K, Cocco L, Martelli AM, Libra M, Candido S, et al. Roles of EGFR and KRAS and their downstream signaling pathways in pancreatic cancer and pancreatic cancer stem cells. Adv Biol Regul 2015;59:65–81, doi:http://dx.doi.org/10.1016/j.jbior.2015.06.003.

[40] Zhang R, Qiao H, Chen S, Chen X, Dou K, Wei L, et al. Berberine reverses lapatinib resistance of HER2-positive breast cancer cells by increasing the level of ROS. Cancer Biol Ther 2016;17:925–34, doi:http://dx.doi.org/10.1080/15384047.2016.1210728.

[41] DeFeo-Jones D, Barnett SF, Fu S, Hancock PJ, Haskell KM, Leander KR, et al. Tumor cell sensitization to apoptotic stimuli by selective inhibition of specific Akt/PKB family members. Mol Cancer Ther 2005;4:271–9.